Synthesis of SFQ Circuits with Compound Gates

Rassul Bairamkulov, Alessandro Tempia Calvino(✉), and Giovanni De Micheli

Integrated Systems Laboratory, EPFL, Lausanne, Switzerland
{rassul.bairamkulov,alessandro.tempiacalvino,giovanni.demicheli}@epfl.ch

Abstract. Rapid single-flux quantum (RSFQ) is one of the most advanced superconducting technologies with the potential to supplement or replace conventional VLSI systems. However, scaling RSFQ systems up to VLSI complexity is challenging due to fundamental differences between RSFQ and CMOS technologies. Due to the pulse-based nature of the technology, RSFQ systems require gate-level pipelining. Moreover, logic gates have an extremely limited driving capacity. Path balancing and clock distribution constitute a major overhead, often doubling the size of circuits. Gate compounding is a novel technique that substantially enriches the functionality realizable within a single clock cycle. However, standard logic synthesis tools do not support its specific synchronization constraints. In this paper, we build first a database of minimum-area compound gates covering all the Boolean functions up to 4 variables and all possible input arrival patterns. Then, we propose a technology mapping method for RSFQ circuits that exploits compound gates using the database as a cell library. We evaluate our framework over the EPFL and ISCAS benchmark circuits. Our results show, on average, a 33% lower logic depth with 24% smaller area, as compared to the state of the art. We further extend our technology mapping framework to support the novel three-input SFQ gates, namely `AND3`, `MAJ3`, and `OR3`. We demonstrate the by using these gates, the area and logic depth of the logic networks are reduced, on average, by 11% and 30% respectively, indicating that developing the logic cells for these three-input gates can significantly improve the scalability of the SFQ technology.

Keywords: Single-Flux Quantum · logic synthesis

1 Introduction

Rapid Single-Flux Quantum (RSFQ) [1] is one of the most promising beyond-CMOS technologies. RSFQ systems consistently achieve operating frequencies on the order of tens of gigahertz [2–4], with particular cells operating at hundreds of gigahertz [5–7]. Furthermore, the operating power of the RSFQ systems is two to three orders of magnitude smaller than CMOS, even considering the refrigeration power [8].

Published by Springer Nature Switzerland AG 2024
I. (Abe) M. Elfadel and L. Albasha (Eds.): VLSI-SoC 2023, IFIP AICT 680, pp. 3–19, 2024.
https://doi.org/10.1007/978-3-031-70947-0_1

However, achieving the aforementioned advantages at scale remains a challenge. Unlike CMOS, most RSFQ logic gates operate as latches with one clock input and one or more data inputs [9]. Arrival of a *single-flux quantum* (SFQ) pulse at the data input changes the internal state of the gate. The presence or absence of an SFQ pulse within the clock period represents logical `1` or `0`, respectively. The clock pulse resets the gate to initial state, potentially releasing an SFQ pulse. This reliance on the clock signal requires SFQ circuits to be pipelined at the gate level. To ensure a correct data propagation, i.e., correct data arrives in the correct time frame, path balancing is required, as shown by the two path-balancing D-flip-flops (DFF) in Fig. 1b. Furthermore, due to the quantized nature of SFQ pulses, most RSFQ primitives have a maximum driving capacity of one gate. Consequently, a special cell called *splitter* is used to duplicate signals [9,10], as illustrated in Fig. 1.

Despite the advances in RSFQ technology mapping [11–13], the number of path-balancing DFFs and splitters can be prohibitively large, degrading the area and yield of an integrated system [14]. Different approaches have been proposed in the literature to tackle this fundamental issue. In [11], the number of path-balancing DFFs is reduced using dynamic programming, yielding, on average a 12% smaller area. Further reductions in path-balancing overhead is achieved by using dual clocking, where high- and low- frequency clock signals are used [15]. This technique however requires relatively expensive NDRO DFFs along with the duplication of the clock distribution network.

Different techniques to reduce the number of clocked elements are proposed in the literature [16,17]. In dynamic SFQ (DSFQ) the gates reset to the initial state after the specified period of time [18]. The design of DSFQ circuits is therefore similar to CMOS circuits where large combinational blocks can be synchronized using relatively few synchronous elements [10]. A similar approach based on clockless logic gates is proposed in [2]. Based on nondestructive readout (NDRO) flip-flops, two additional clockless cells, namely the `NIMPLY` ($\neg x_0 \wedge x_1$) and the `AND` functions, are efficiently realized using fewer clocked elements for synchronization. The advantages of these approaches are smaller area, lower clock network complexity, and simpler path balancing, as compared to conventional RSFQ. The timing constraints, however, constitute a major challenge. In DSFQ, the interaction between the input skew tolerance, clock frequency, and bias margins [10]

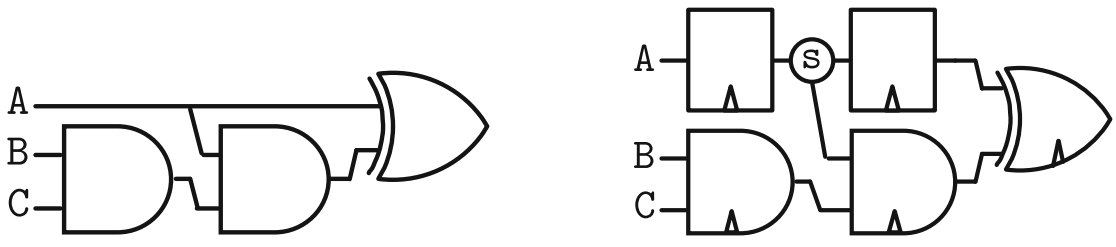

a) b)

Fig. 1. a) An example of a CMOS circuit. b) Equivalent RSFQ circuit with a splitter and two path-balancing DFFs.

complicates the circuit design. The NDRO-based clockless gates are particularly sensitive to the arrival time of the inputs, necessitating careful timing analysis [19].

The *gate compounding* technique has been recently proposed as an alternative strategy to reduce the number of clocked elements [20]. Unlike DSFQ and clockless gates, *compound gates* (logic gates obtained by gate compounding) are not sensitive to the arrival of the inputs, reducing the complexity of the system design process. The functionality achievable within a single clock cycle is enriched by exploiting RSFQ synchronization mechanisms. Gate compounding can significantly reduce the pipeline depth and number of clocked elements, not only improving the latency and area of a functional circuit, but also reducing the size of the clock distribution network. However, due to complex synchronization requirements, traditional technology mapping tools are not directly applicable.

In this work, we first summarize a technology mapping method for SFQ compound gates based on a previous paper [21]. Inspired by [22–24], we create a database of compound gates using enumeration. We generate functionally correct and area-optimal compound gates for all functions up to four variables and all possible input arrival patterns. Next, we utilize these gates as library cells during technology mapping to synthesize large-scale SFQ circuits. Furthermore, we extend this framework to leverage three-input threshold SFQ gates (`AND3`, `MAJ3`, and `OR3`) as additional primitives for the creation of compound gates. In the experimental results, we show a drastic reduction in the area and logic depth by 24% and 33%, respectively, compared to the state-of-the-art, when using compound gates based on 2-input cell primitives. When extending compound gates to use 3-input cell primitives, the area and logic depth are further reduced by 11% and 30%, respectively, compared to compound gates generated using 2-input cells.

2 Gate Compounding Technique

The gate compounding technique exploits differences in pulse synchronization mechanisms to reduce the pipeline depth of an RSFQ circuit. In particular, RSFQ logic gates can be divided into three categories, namely, *AA*, *AS*, and *SA*, where the first letter denotes whether input signals should arrive (a)synchronously, while the second letter indicates whether the output is released (a)synchronously.

AA elements process the inputs immediately upon arrival and the output is released without a synchronizing signal (clock). For instance, a *merger* cell, often referred to as *confluence buffer* (CB), directs signals from multiple (typically two) input branches into one output branch, i.e., implements an `OR` function. Note that the merger produces two subsequent output pulses if input pulses are temporally separated, or a single pulse, if input signals arrive simultaneously.

AS elements process the input information immediately upon arrival and release the output synchronously after the arrival of the clock signal. The simplest RSFQ component of this type is *D-flip-flop (DFF)* that stores an incoming pulse and releases it upon the arrival of the clock signal. Other important AS elements are the *inverter* (`NOT`) and *exclusive-or* (`XOR`).

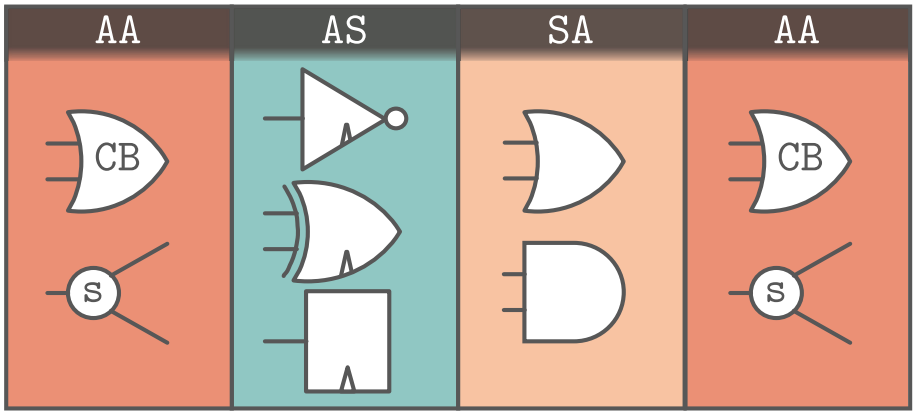

Fig. 2. Generic compound gate structure.

SA elements require the inputs to arrive simultaneously. The result of the computation is released immediately after processing. Assuming inputs arrive simultaneously, a CB can be tuned to produce at most a single output pulse, producing an *OR* element [25]. Furthermore, by adjusting the JJ size and bias current, the OR structure can be transformed into AND element. Note that, unlike conventional RSFQ, OR and AND elements are not clocked and require inputs to arrive simultaneously.

These three categories of components govern the flow of data within an RSFQ circuit. Most importantly, the SA components ensure simultaneous release of the SFQ pulses. Therefore, SA components can only be placed directly after the AS elements. To comply with these restrictions, the *gate compounding* technique was proposed in [20]. A compound SFQ logic gate can be produced by following the generic structure illustrated in Fig. 2. Inputs to a compound gate are initially processed by AA elements. The signals then flow towards the AS components where the result of a logical operation is stored until the arrival of the clock signal. The clock signal triggers the simultaneous release of the data towards the SA elements. Finally, the AA components complete the function.

The proposed structure offers two major advantages. Since the initial processing is handled by the AA or AS elements, arbitrary order of input arrival is supported, relaxing the timing constraints of the circuit. The proposed gate compounding technique significantly expands the set of functions realizable within a single clock cycle. Using compound gates, for example, all 16 two-input functions are realized within a single clock cycle, as compared to only 13 functions in conventional SFQ [20].

3 Background and Notation

A multi-output Boolean function $f : \mathbb{B}^k \mapsto \mathbb{B}^m$ maps k input signals to m output signals. A single output Boolean function ($m = 1$) $f : \mathbb{B}^k \mapsto \mathbb{B}$ can be represented as a truth table with 2^k rows. A truth table can be conveniently encoded as a

2^k-bit string $\mathtt{Y} = \overline{\mathtt{y}_{2^k-1} \dots \mathtt{y}_0}$ where bit $\mathtt{y}_i$ denotes the output at the i^{th} row in the truth table. For example, $f_1(\mathtt{x}_1, \mathtt{x}_0) = \mathtt{x}_1 \oplus \mathtt{x}_0$ is encoded as $\mathtt{Y}_1 = \mathtt{0110}_2$, since $f_1(\mathtt{1},\mathtt{1}) = \mathtt{0}$, $f_1(\mathtt{1},\mathtt{0}) = \mathtt{1}$, $f_1(\mathtt{0},\mathtt{1}) = \mathtt{1}$, and $f_1(\mathtt{0},\mathtt{0}) = \mathtt{0}$.

A *Boolean function*[1] f can be represented by a *Boolean network*[2] $\mathcal{N} = (\mathcal{V} = \mathcal{I} \cup \mathcal{O} \cup \mathcal{G}, \mathcal{E})$—a directed acyclic graph (DAG) representing the sequence of the Boolean operations applied to realize f. Set $\mathcal{G}$ is a set of gates, where each node $u \in \mathcal{G}$ applies a function f_u to its *fanins* $FI(u)$ and passes the result to *fanouts* $FO(u)$. Set $\mathcal{I}$ denotes the set of *primary inputs* (PI), i.e., nodes without fanins. Set $\mathcal{O}$ denotes the set of *primary outputs* (PO), i.e., nodes without fanouts.

3.1 Delay

In SFQ, the delay is typically expressed in terms of the number of clock cycles required to realize a function. In practice, input signals can often arrive at different clock cycles, as illustrated in Fig. 3a. We define the *input level pattern* $\boldsymbol{\ell}_{\mathcal{N}} = \left[\ell^0, \dots, \ell^{k-1}\right]$ as a vector of integers describing the clock cycles during which the PI signals enter the network $\mathcal{N}$. Without loss of generality, we normalize the input patterns such that the earliest PI signal arrives at cycle 0, i.e., $\min(\boldsymbol{\ell}_N) = 0$. For example, an input level pattern $\boldsymbol{\ell}_{\mathcal{N}} = [0, 1]$ indicates that the data from the second PI is delayed by one clock cycle. A *level* l_u denotes the number of clock cycles between the earliest PI and node u. The *input arrival pattern* $\mathbf{d}_u = \left[d_u^0 \dots d_u^{k-1}\right]$ is the number of clock cycles between u and each PI,

$$\mathbf{d}_u = [l_u - \ell^0, \dots, l_u - \ell^{k-1}].$$

We define two operators to compare the delay patterns of any two nodes u and v:

$$\mathbf{d}_u = \mathbf{d}_v \Leftrightarrow \forall i \; d_u^i = d_v^i,$$
$$\mathbf{d}_u < \mathbf{d}_v \Leftrightarrow \exists i \; d_u^i < d_v^i \text{ and } \nexists i \; d_u^i > d_v^i.$$

In the former case, corresponding delays are equal. In the latter case, the delays of u are not greater than the corresponding delays of v, but for at least one PI the delay of u is smaller.

3.2 Cost

The most common metric to evaluate the cost of an SFQ circuit is the JJ count, which directly correlates with the area of an SFQ circuit. Let q_u be the area cost associated with the logic primitive implemented by a node u. The area cost $c(\mathcal{N})$ of a circuit $\mathcal{N}$ is the sum of costs q_u for each node $u \in \mathcal{G}$. A transitive fanin cone $TFI(u)$ is defined as the set of all nodes having a path to u. The area cost c_u of a node u is defined as the cost of its TFI. Note that c_u differs from q_u,

[1] For brevity, we use the term *function* to represent a *Boolean function*.
[2] We use the terms *network* and *circuit* to represent a *Boolean network*.

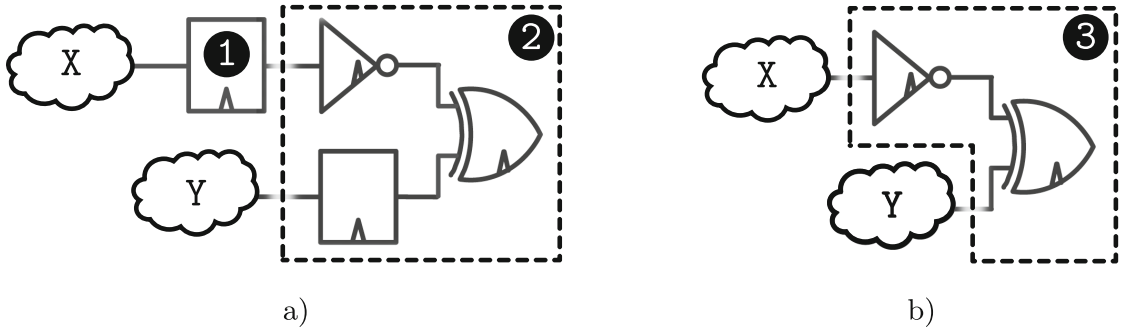

a) b)

Fig. 3. Realization of an `XNOR` function between networks `X` and `Y`. The left network uses a path-balancing DFF (`1`) followed by an `XNOR` with equal delay pattern (`2`). This structure requires three clock cycles and 33 JJs. The right network uses an `XNOR` element with unequal delay pattern (`3`), requiring two clock cycles and 21 JJs.

since q_u defines the cost of a single primitive, while c_u is the sum of costs of all ancestors of u. Suppose nodes u, v are fanins of node w. The cost of the node w is,

$$c_w = q_w + S(u, v),$$

$$S(u, v) = \sum_{n \in TFI(u) \cup TFI(v)} \left[q_n + q_s \max\left(|FO(n)| - 1, 0 \right) \right],$$

where q_s is the cost of splitter.

An SFQ circuit should comply with specific technological constrains, such as path balancing and fanout constraints in SFQ. With SFQ gate compounding, gates also follow the structure described in Fig. 2 to avoid the data hazards described in the upcoming subsection.

3.3 Data Hazards

Double Pulse Hazard. If two pulses entering a CB are sufficiently spaced in time, two subsequent SFQ pulses are generated at the output, potentially producing an error. For instance, a double pulse produced by a CB entering a `XOR` may trigger unwanted switching, producing incorrect result. In particular, the internal storage loop within a `XOR` is toggled one additional time between `0` or `1` by the input pulses. Nevertheless, if the CB has its output pin connected to a DFF or an inverter, the second pulse has no effect on the system [9].

Consider the circuit implementing $(A \vee B) \oplus C$ shown in Fig. 4. The storage loop within the `XOR` element is correctly switched and reset with pulses `A` and `C`. The pulse `B`, however, sets the storage loop to state `1`, producing an incorrect result. To avoid this data hazard, the `XOR` component is placed after a CB only if the CB is guaranteed to produce at most one SFQ pulse, i.e., the inputs to a CB are never simultaneously equal to `1`.

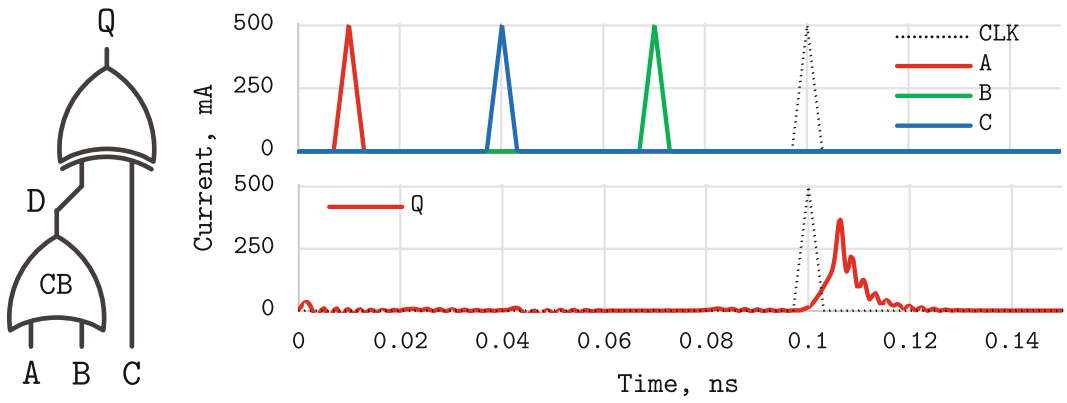

Fig. 4. Incorrect realization of $(\mathtt{A} \vee \mathtt{B}) \oplus \mathtt{C}$ function using a CB and an XOR. The main loop within an XOR element is set to 1 by A, reset to 0 by C, and subsequently set to 1 by pulse B, incorrectly producing an output pulse.

To identify the condition where a CB can produce two pulses, we assign a hazard flag $\mathtt{h}_n$ to each node n. If n is not a CB, $\mathtt{h}_n$ is 0; otherwise,

$$\mathtt{h}_n = \mathtt{h}_u \vee \mathtt{h}_v \vee \delta(\mathtt{Y}_u \wedge \mathtt{Y}_v),$$

where $u, v \in FI(n)$ and $\delta(\mathtt{Y}) = 1$ only if Y is nonzero.

For example, consider nodes u, v, w, with $\mathtt{Y}_u = 1010_2$, $\mathtt{Y}_v = 0001_2$, $\mathtt{Y}_w = 1100_2$, and $\mathtt{h}_u = \mathtt{h}_v = \mathtt{h}_w = 0$. Connecting u and v to a CB produces node p that can be used with XOR, since $\mathtt{h}_u = \mathtt{h}_v = 0$ and

$$\delta(\mathtt{Y}_u \wedge \mathtt{Y}_v) = \delta(1010_2 \wedge 0001_2) = \delta(0000_2) = 0 \Rightarrow \mathtt{h}_p = 0,$$

i.e., the u and v are never simultaneously equal to 1. In contrast, connecting u and w to a CB produces node q that cannot be used with XOR, since

$$\delta(\mathtt{Y}_p \wedge \mathtt{Y}_w) = \delta(1010_2 \wedge 1100_2) = \delta(1000_2) = 1 \Rightarrow \mathtt{h}_q = 1.$$

Suppose node r is produced by connecting q and v to a CB. Although $\delta(\mathtt{Y}_q \wedge \mathtt{Y}_v) = 0$, node r cannot be used with XOR since $\mathtt{h}_q = 1 \Rightarrow \mathtt{h}_r = 1$.

Desynchronization Hazard. The signal desynchronization is a timing hazard where the inputs cannot simultaneously arrive to an SA element. Consider for example the circuit illustrated in Fig. 5a. The splitter is placed between the AS (DFF) and SA (AND) components. Delays $a_0 \to a_1$ and $b_0 \to b_1$ are not equal. Therefore, pulses from A and B do not arrive simultaneously, violating the input timing requirement of the AND element. Thus, the AND operates as a constant 0.

A possible correction is shown in Fig. 5b. The splitter is placed before the DFFs to equalize delays $a_0 \to a_1$ and $b_0 \to b_1$. The timing violation is therefore avoided at the cost of an additional DFF.

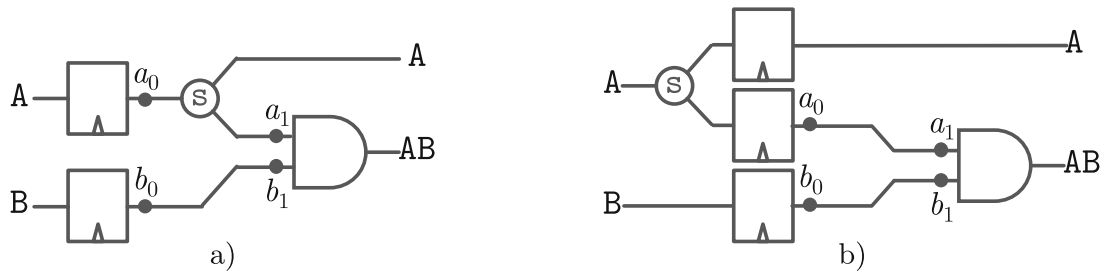

Fig. 5. a) A system violating the compound gate structure. Any AA element (splitter) between AS (DFF) and SA (AND) elements may desynchronize the input arrival. b) The issue is resolved by moving the splitter before the AS elements.

4 Library Construction

The fixed structure of the compound gates combined with the hazards described in the previous section complicates the technology mapping process. For example, AA elements should be prevented from being placed between AS and SA elements, an issue described in Sect. 3.3. Adapting the existing tools to consider these constraints requires to significantly modify the underlying algorithms, potentially degrading run time and quality of results.

Area- or delay-optimal SFQ circuits can be created using exact synthesis methods, such as Boolean satisfiability [26,27] and enumeration [22]. However, exact methods are limited to small sizes (≤ 16 nodes) and few variables (≤ 6), due to the computational intractability of the problem. Nevertheless, exact synthesis can be applied to create a database of optimal small-scale structures. Since the number of Boolean functions grows double exponentially with the number of variables (2^{2^k}), complete databases are typically limited to 4 variables. These locally-optimal networks are subsequently used to produce larger networks [22–24]. Library-driven approaches have been successfully applied to MIG resynthesis [23,24] and AQFP logic synthesis [22]. The database-driven mapping offers several advantages:

- *Functional correctness.* Each circuit block within a database describes a realization of a logic function complying with the specific technological constraints. Thus, technology mapping can safely proceed at the block level, since the technological requirements are satisfied during the database creation.
- *Local optimality.* The logic blocks in the database can be optimized for area or delay.
- *Performance.* The parameters of each logic block, such as area and delay, are computed in advance and can be accessed in constant time during mapping.
- *Reuse.* Once created, the database can be used multiple times to synthesize arbitrary SFQ circuits.

In this section, we present the procedure to create a database of area-optimal compound gate structures for each of the k-input, single-output Boolean function.

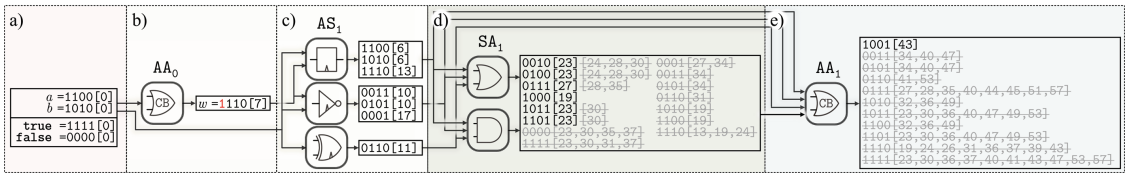

Fig. 6. Example of enumeration with 2 primary inputs represented by truth tables `1100` and `1010`. The numbers in brackets represent the cost of a node (in JJ). The red `1` represents the double pulse hazard. The crossed grey numbers represent the discarded truth tables. (Color figure online)

4.1 Enumeration Procedure

The algorithm constructs a Boolean network $\mathcal{N} = (\mathcal{V}, \mathcal{E})$, where nodes represent a particular realization of a logic function using compound gates. Each node $u = (\mathtt{Y}_u, l_u, c_u, \mathtt{h}_u) \in V$ is a 4-tuple of a truth table, level, cost, and hazard flag. The procedure is initialized with k nodes representing the PIs. For example, Fig. 6a describes the initialization for $k = 2$:

$$a = (\mathtt{1100}_2, 0, 0, \mathtt{0}) \qquad b = (\mathtt{1010}_2, 0, 0, \mathtt{0})$$

For completeness, constant `true` and `false` are also included. After initialization, the algorithm cycles through three subroutines, following the compound gate structure in Fig. 2.

AA. The stage $\mathtt{AA}_i$ implements the addition of AA elements to a compound gate at level i. For each pair of nodes $u = (\mathtt{Y}_u, i, c_u, \mathtt{h}_u)$ and $v = (\mathtt{Y}_v, i, c_v, \mathtt{h}_u)$, a new node $w = (\mathtt{Y}_u \vee \mathtt{Y}_v, i, q_{\mathtt{CB}} + S(c_u, c_v), \mathtt{h}_w)$ is produced. Consider the $\mathtt{AA}_1$ stage, illustrated in Fig. 6b, where the new node $w = (\mathtt{1110}_2, 0, 7, \mathtt{1})$ is discovered. The 7-JJ cost of the node is the cost of a CB used to realize this function.

AS. For each node $u = (\mathtt{Y}_u, i-1, c_u, \mathtt{h}_u)$, stage $\mathtt{AS}_i$ produces two new nodes,

$$p = (\mathtt{Y}_u, i, c_u + c_{\mathtt{DFF}}, \mathtt{0}) \quad \text{and} \quad q = (\neg\mathtt{Y}_u, i, c_u + c_{\mathtt{NOT}}, \mathtt{0}),$$

corresponding to addition of a DFF and `NOT` element. Note that the hazard flag is reset to `0`, since only a single pulse is produced by the AS elements. In addition, for each pair of nodes $u = (\mathtt{Y}_u, i-1, c_u, \mathtt{0})$ and $v = (\mathtt{Y}_v, i-1, c_v, \mathtt{0})$, whose hazard flag is `0`, a new node is produced

$$r = (\mathtt{Y}_u \oplus \mathtt{Y}_v, i, q_{\mathtt{XOR}} + S(c_u, c_v), \mathtt{0}).$$

In Fig. 6c, three new nodes are produced by a DFF, while four new truth tables are discovered by applying `NOT` and `XOR` operations. Note that the node w is not used with `XOR` due to the hazard flag $\mathtt{h}_w = 1$.

SA. After the AS stage, inputs are synchronized enabling the use of SA gates. At stage $\texttt{SA}_i$, each pair of nodes $u = (\texttt{Y}_u, i, c_u, \texttt{0})$ and $v = (\texttt{Y}_v, i, c_v, \texttt{0})$ produces 2 new nodes

$$p = (\texttt{Y}_u \wedge \texttt{Y}_v, i, q_{\texttt{AND}} + S(c_u, c_v), \texttt{0}), \text{ and}$$
$$q = (\texttt{Y}_u \vee \texttt{Y}_v, i, q_{\texttt{OR}} + S(c_u, c_v), \texttt{0}).$$

In Fig. 6d, the outputs of the $\texttt{AS}_1$ stage proceed to the $\texttt{SA}_1$ stage where the logical AND and OR are applied to the outputs of the previous stage. The 6 nodes implementing previously undiscovered functions with smallest cost are added to the network, while 36 nodes are discarded.

The algorithm repeats these three stages ($\texttt{AA}_{i-1} \to \texttt{AS}_i \to \texttt{SA}_i \to \texttt{AA}_i \to \ldots$) until all 2^{2^k} k-input functions are realized. In our example for $k = 2$, after stage $\texttt{SA}_1$ the algorithm proceeds to stage $\texttt{AA}_1$, where 78 nodes are produced, of which only a single node implements the remaining function $\texttt{1001}_2$. After this stage, all of the $2^{2^2} = 16$ two-input truth tables are discovered and the enumeration process is terminated.

4.2 Filtering

During the enumeration process, the size of the network grows rapidly with each additional stage. In Fig. 6, for example, only 7 nodes are produced at stage $\texttt{AS}_1$, while 62 nodes are produced at stage $\texttt{AA}_1$. The number of nodes considered during enumeration drastically increases with k, with several billions of nodes processed while enumerating four-input functions. To limit the number of nodes and prevent inferior nodes from being added to the database, the dominance relationship is used. Suppose, the node u implements a Boolean function f with input arrival pattern $\mathbf{d}_u$ and area c_u. Also, suppose another node v implementing the same function f with input arrival pattern $\mathbf{d}_v$ and area c_v has previously been discovered. The node v is said to *dominate* the node u in two cases,

- faster delay: $\mathbf{d}_v < \mathbf{d}_u$ and $c_v \leq c_u$;
- lower cost: $\mathbf{d}_v = \mathbf{d}_u$ and $c_v < c_u$.

In these cases, the node u is not created.

4.3 Input Arrival Patterns

During initial enumeration, all PIs are placed at equal levels $\boldsymbol{\ell} = (0, \ldots, 0)$. To consider different input arrival patterns, the enumeration process is repeated with PIs introduced at different levels $\boldsymbol{\ell} = (\ell^0, \ldots, \ell^{k-1})$. The number of input level patterns considered during the enumeration process can be reduced based on dominance relationship. Suppose that, while considering the pattern $\boldsymbol{\ell}_a = (\ell^1, \ldots, \ell^q, \ldots, \ell^k)$, all nodes were dominated by or equivalent to previously discovered nodes. The pattern $\boldsymbol{\ell}_b = (\ell^1, \ldots, \ell^q + 1, \ldots, \ell^k)$ is therefore unlikely to yield a non-dominated node, due to inferior delay and cost.

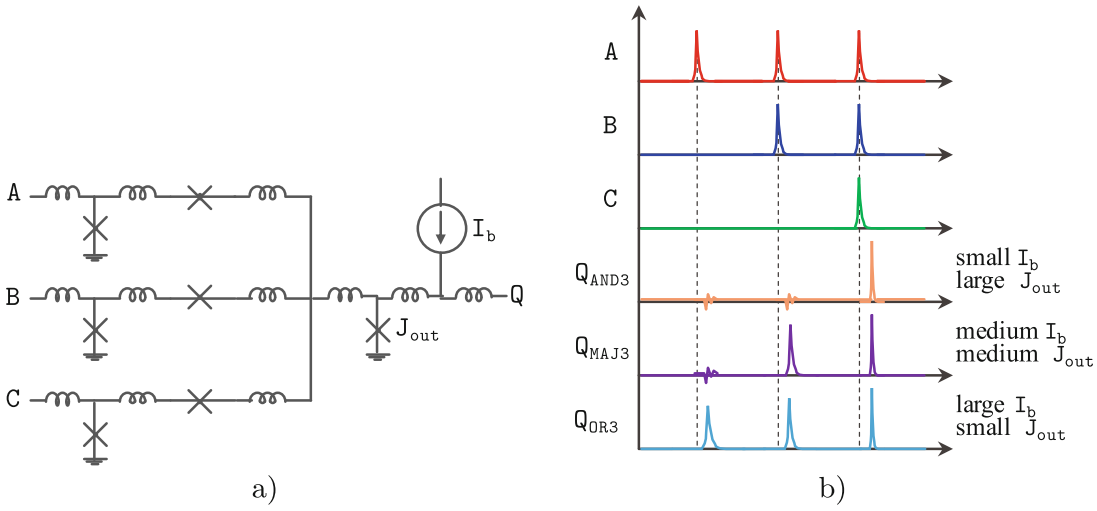

Fig. 7. Circuit and waveforms of the three-input threshold SFQ gates. a) Circuit diagram. b) Waveforms. By increasing the bias current and reducing the size of junction J_{out}, the AND3 gate can be turned into MAJ3 and OR3.

5 Extension to Three-Input Gates

Multiple works in the literature describe the use of the gates with fanin higher than two [28,29]. In the pioneering work [29], the ternary majority (MAJ3) function has been shown to provide greater expressive power, producing networks with superior area and delay. The high expressive power of the three input gates has been further investigated in [28]. Generally, three-input gates lead to a significant reduction in the number of necessary gates to implement a network, but it also increases the overall edge count. Multi-input gates in SFQ technology have been discussed in [30], where AND and OR gates with up to five inputs have been designed. Three-input majority gates for SFQ technology have been proposed in [31].

The topology of the SFQ AND3, MAJ3, and OR3 gates is a natural extension of the two-input AND2 and OR2 structures, as illustrated in Figs. 7a-b. The SFQ AND2 and OR2 gates can be viewed as threshold logic functions. In AND2 gate, the bias current is reduced while the size of the output junction is increased. Therefore, two pulses should arrive simultaneously from each input branch to produce and output pulse. By increasing the bias current and reducing the size, the output junction is made more sensitive, producing an OR2 gate. A single pulse is sufficient to switch the output junction.

By adding an extra input branch to the AND2/OR2 topology, the three-input threshold gates can be realized. The AND3 gate is produced by setting the small bias current and large output junction size. SFQ pulses from all three branches are necessary to switch the output junction. By increasing the bias current and reducing the size of the output the gate becomes MAJ3, and next OR3, requiring, respectively two and one pulse to switch the output junction, as shown in Fig. 7c.

To evaluate the impact of using the three-input gates in SFQ logic synthesis, we created a separate database incorporating the `AND3`, `MAJ3`, and `OR3` gates. From the synchronization perspective, these gates belong to the SA category, since they require all inputs to arrive simultaneously. The enumeration process follows the same procedures outlined in Sects. 4.1–4.3.

6 Technology Mapping

We propose a three-stage technology mapping flow to synthesize arbitrary Boolean networks using SFQ compound gates, similarly to [13]. First, we employ a delay-driven technology mapper that uses the computed database as a cell library. Due to path balancing, delay optimization is essential for area reduction in SFQ circuits. Intuitively, longer critical paths require more DFF elements due to longer paths to balance [32].

Next, our flow inserts path-balancing DFFs and minimizes their number using minimum-area retiming [33], which provides an optimal solution. Note that retiming preserves the path-balancing constraint since each path traverses the same number of DFFs before and after retiming.

Finally, splitter cells are inserted to satisfy the driving capacity constraint. Our synthesis flow has been implemented using the open-source logic synthesis library `mockturtle` [34].

7 Experimental Results

7.1 Database Creation

We employed a computing cluster with 48 2.5 GHz Intel Xeon E5-2680 CPUs and 256 GB of RAM to create two databases. The original database only considers gates with up to two inputs. The extended database incorporates the three-input threshold gates, namely `AND3`, `MAJ3`, and `OR3`. Due to the computational complexity, we limited the number of inputs to four, i.e., $k = 4$. The enumeration process starts from pattern $\boldsymbol{\ell}_0 = (0, 0, 0, 0)$, i.e., all of the PIs are at the same level. During the subsequent iterations, the level of one of the PIs is incremented and the enumeration process is repeated. If the enumeration does yield to non-dominated nodes, a new PI level is incremented. Figure 8 illustrates possible level patterns considered by the enumeration process.

For the original database, the computation for the input level pattern $\boldsymbol{\ell}_0 = (0, 0, 0, 0)$ (without the three-input gates) required seven hours, evaluating over 13 billion nodes. Other delay patterns required between one to five hours. The resulting database was created in 52 h and consisted of 488,636 entries. Next, we filtered entries based on input-permutation equivalences (P-classes) [35]. Our final database contains 28,258 non-dominated implementations for all the 3,984 P-classes of Boolean functions up to 4 variables. Each entry represents a valid RSFQ compound gate. Note again that the considerable initial runtime for database creation is amortized by repeated use.

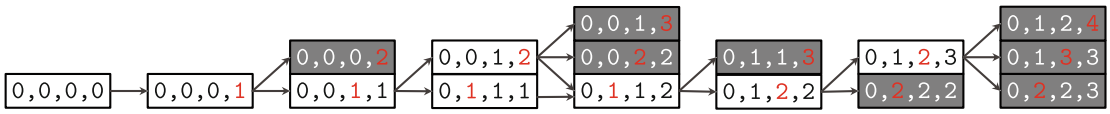

Fig. 8. Level patterns considered during enumeration. Due to permutation symmetry, only the sorted level patterns are considered. The process starts with the pattern $(0, 0, 0, 0)$. In subsequent iterations, the level of one of the PIs is incremented (marked red). If the iteration does not yield any cost- or area-optimal nodes, the pattern is not incremented (shaded gray). (Color figure online)

The process of calculating the extended database requires much smaller runtime as compared to the two-input database. The initial input level pattern $\ell_0 = (0, 0, 0, 0)$ required less than three hours while each remaining input arrival pattern was explored in 1–2 hours. This speedup is attributed to the high expressive power of the three-input gates. During the enumeration process, the depth-optimal implementations of all $2^{2^4} = 65,536$ functions are found with fewer logic levels and nodes to be explored.

7.2 Mapping with Original Database

We apply our original database to synthesize a subset of EPFL [34] and ISCAS [36] benchmark circuits. We compare our results against PBMap [11], the state-of-the-art dynamic programming algorithm for path balancing. The results are shown in Table 1. Compared to the state of the art, gate compounding technique drastically reduces logic depth by an average of 33%. Due to the use of more expressive compound gates, the area of the circuits (expressed as total JJ count) is reduced by an average of 24%, despite 53% larger number of path-balancing DFFs.

Despite substantial improvements in many benchmarks, our approach yields a weaker result in `dec` circuit. The increase in JJ count can be attributed to two factors. First, the logic depth of this circuit is only 4 cycles, limiting the impact of compound gates. Second, the JJ cost of each primitive in the RSFQ library used in [11] is not openly available at the reference. Likely, the CONNECT cell library [37] used in this work has a higher JJ cost for logic primitives compared to [11], contributing to the area increase.

We also compare our results with the dual clock methodology [15]. A logic circuit is partitioned into separate clocking domains using the NDRO flip flops. Subcircuits within each partition are clocked at high frequency, while the NDRO flip flops operate at a frequency 7 times smaller than the high frequency. The throughput of the system is therefore reduced by a factor of 7. The results are compared in Table 2. Despite 7 times smaller throughput and 64% fewer DFFs, the dual clocking method requires almost 2 times more JJs as compared to gate compounding. In addition, DCM systems require relatively expensive NDRO DFFs, pulse repeaters and an additional low-frequency clock distribution network, further degrading the area of the system.

Table 1. Number of path-balancing DFFs, JJs, and logic depth in a subset of EPFL [38] and ISCAS [36] benchmarks

Benchmark	#DFF			#JJ			Delay			Runtime, s
	Baseline	Ours	Ratio	Baseline	Ours	Ratio	Baseline	Ours	Ratio	
`sin`	13,666	17,627	1.29	215,318	126,694	0.59	182	86	0.47	0.399
`cavlc`	522	987	1.89	16,339	15,098	0.92	17	11	0.65	0.009
`dec`	8	16	2.00	5,469	6,324	1.16	4	4	1.00	0.006
`int2float`	270	443	1.64	6,432	5,616	0.87	16	10	0.63	0.004
`priority`	9,064	14,754	1.63	102,085	95,370	0.93	127	125	0.98	0.013
`c499`	476	512	1.08	7,758	5,593	0.72	13	8	0.62	0.040
`c880`	774	1,179	1.52	12,909	8,359	0.65	22	13	0.59	0.013
`c1908`	696	799	1.15	12,013	5,553	0.46	20	11	0.55	0.025
`c3540`	1,159	1,556	1.34	28,300	22,231	0.79	31	18	0.58	0.034
`c5315`	2,908	3,727	1.28	52,033	33,524	0.64	23	13	0.57	0.091
`c7552`	2,429	4,744	1.95	48,482	28,900	0.60	19	13	0.68	0.115
Average			1.53			0.76			0.67	

Table 2. Comparison with DCM [15] with 1/7 throughput on a subset of EPFL [38] and ISCAS [36] benchmarks

benchmark	DCM (1/7) [15]		Our Work			
	#DFF	#JJ	#DFF	Ratio	#JJ	Ratio
`int2float`	117	7,770	440	3.76	5,973	0.77
`priority`	8,562	257,252	14,754	1.72	68,177	0.27
`voter`	7,204	447,044	8,357	1.16	189,622	0.42
`c432`	224	10,734	1,180	5.27	6,905	0.64
`c880`	362	14,658	1,176	3.25	8,650	0.59
`c1355`	193	8,739	448	2.32	5,703	0.65
`c1908`	282	13,169	799	2.83	5,497	0.42
`c3540`	776	43,437	1,554	2.00	20,820	0.48
Average				2.79		0.53

7.3 Mapping Using Three-Input Gates

To evaluate the effect of using three-input gates in SFQ logic synthesis, we repeat our experiments using the extended database. The results are shown in Table 3. On average, the use of three-input gates reduces the number of DFFs by 43%, while reducing the area by 11%. These improvements can be attributed to two factors. First, the compound gates utilizing three-input elements, provide more logical expressive power with smaller area. Furthermore, the logic depth of the networks in reduced by 30%. With smaller logic depth fewer path balancing DFFs are needed to realize the same function.

Table 3. Synthesis of a subset of EPFL [38] and ISCAS [36] benchmarks using the original and extended (with three input-gates) databases

Benchmark	#DFF			#JJ			Delay		
	Original	Extended	Ratio	Original	Extended	Ratio	Original	Extended	Ratio
`sin`	17,627	11,988	0.680	126,694	105,377	0.832	86	69	0.802
`cavlc`	987	433	0.439	15,098	13,311	0.882	11	7	0.636
`dec`	16	2	0.125	6,324	8,848	1.399	4	2	0.500
`int2float`	443	182	0.410	5,616	4,521	0.805	10	6	0.600
`priority`	14,754	10,084	0.683	95,370	44,016	0.462	125	62	0.496
`c499`	512	430	0.840	5,593	4,847	0.867	8	7	0.875
`c880`	1,179	780	0.662	8,359	7,283	0.871	13	10	0.769
`c1908`	799	435	0.544	5,553	5,667	1.021	11	8	0.727
`c3540`	1,556	936	0.602	22,231	19,131	0.861	18	13	0.722
`c5315`	3,727	2,798	0.751	33,524	31,139	0.929	13	11	0.846
`c7552`	4,744	2,201	0.464	28,900	25,084	0.868	13	9	0.692
Average			0.564			0.891			0.697

8 Conclusions

RSFQ technology has the potential to enhance power and speed of the mainstream computing systems by several orders of magnitude. The gate compounding technique is a novel method to reduce the logic depth by exploiting the synchronization mechanisms of RSFQ technology. With more expressive logic gates, area of the circuits is considerably reduced. In this paper, we proposed a scalable technology mapping method that leverages SFQ compound gates. We generated a database of functionally correct and area-optimal compound gates for all functions up to 4 variables. Then, we applied a delay-driven technology mapping using the pre-computed database as a cell library. In the experimental results, we showed a substantial reduction in the area and logic depth by 24% and 33%, respectively, compared to the state-of-the-art.

We further extend our results to support the logic synthesis with three-input threshold gates, namely `AND3`, `MAJ3`, and `OR3`. By using the more expressive logic gates, the area and logic depth is further reduced by, respectively, 11% and 30%. These results indicate the great potential for the use of these three-input gate in SFQ logic synthesis, motivating the development of these logic cells in future SFQ cell libraries.

Acknowledgement. This research was supported by the SNF grant "Supercool: Design methods and tools for superconducting electronics", 200021_1920981, and Synopsys Inc.

References

1. Likharev, K., Mukhanov, O., Semenov, V.: Resistive single flux quantum logic for the josephson-junction digital technology. In: Proceedings of International Conference on Superconducting Quantum Devices, vol. 85, pp. 1103–1108 (1985)
2. Kawaguchi, T., Tanaka, M., Takagi, K., Takagi, N.: Demonstration of an 8-bit SFQ carry look-ahead adder using clockless logic cells. In: International Superconductive Electronics Conference (2015)
3. Gupta, D., Inamdar, A.A., Kirichenko, D.E., Kadin, A.M., Mukhanov, O.A.: Superconductor analog-to-digital converters and their applications. In: Proceedings of IEEE MTT-S International Microwave Symposium (2011)
4. Yang, S., Gao, X., Yang, R., Ren, J., Wang, Z.: A hybrid josephson transmission line and passive transmission line routing framework for single flux quantum logic. IEEE TASC **32**(9), 1–11 (2022)
5. Chen, W., Rylyakov, A., Patel, V., Lukens, J., Likharev, K.: Rapid single flux quantum t-flip flop operating up to 770 GHz. IEEE TASC **9**(2), 3212–3215 (1999)
6. Herr, Q.P., Smith, A.D., Wire, M.S.: High speed data link between digital superconductor chips. Appl. Phys. Lett. **80**(17), 3210–3212 (2002)
7. Akaike, H., et al.: Demonstration of a 120 GHz single-flux-quantum shift register circuit based on a 10 kA cm^{-2} Nb process. Supercond. Sci. Technol. **19**(5), S320 (2006)
8. Holmes, D.S., Ripple, A.L., Manheimer, M.A.: Energy-efficient superconducting computing-power budgets and requirements. IEEE TASC **23**(3), 1701610 (2013)
9. Bunyk, P., Likharev, K., Zinoviev, D.: RSFQ technology: physics and devices. Int. J. High Speed Electron. Syst. **11**(01), 257–305 (2001)
10. Krylov, G., Friedman, E.G.: Single Flux Quantum Integrated Circuit Design. Springer, Cham (2022)
11. Pasandi, G., Pedram, M.: PBMap: a path balancing technology mapping algorithm for single flux quantum logic circuits. IEEE TASC **29**(4), 1–14 (2019)
12. Kito, N., Takagi, K., Takagi, N.: Logic-depth-aware technology mapping method for RSFQ logic circuits with special RSFQ gates. IEEE TASC **32**(4), 1–5 (2021)
13. Calvino, A.T., De Micheli, G.: Algebraic and boolean methods for SFQ superconducting circuits. In: Proceedings of ASP-DAC (2024)
14. Bairamkulov, R., Jabbari, T., Friedman, E.G.: QuCTS - single-flux quantum clock tree synthesis. IEEE TCAD **41**(10), 3346–3358 (2022)
15. Pasandi, G., Pedram, M.: Depth-bounded graph partitioning algorithm and dual clocking method for realization of superconducting SFQ circuits. ACM JETCAS **17**(1), 1–22 (2020)
16. Yang, J.-H., et al.: Distributed self-clock: a suitable architecture for SFQ circuits. IEEE TASC **30**(7), 1–7 (2020)
17. Li, X., et al.: Optimization of delay time stabilization for single flux quantum cell library. IEEE TASC **30**(7), 1–5 (2020)
18. Rylov, S.V.: Clockless dynamic SFQ and gate with high input skew tolerance. IEEE TASC **29**(5), 1–5 (2019)
19. Kawaguchi, T., Takagi, K., Takagi, N.: Static timing analysis for single-flux-quantum circuits composed of various gates. IEEE TASC **32**(5), 1–9 (2022)
20. Bairamkulov, R., De Micheli, G.: Compound logic gates for pipeline depth minimization in single flux quantum integrated systems. In: Proceedings of GLSVLSI (2023)

21. Bairamkulov, R., Calvino, A.T., De Micheli, G.: Synthesis of SFQ circuits with compound gates. In: 2023 IFIP/IEEE 31st International Conference on Very Large Scale Integration (VLSI-SoC), pp. 1–6 (2023)
22. Marakkalage, D.S., Riener, H., De Micheli, G.: Optimizing adiabatic quantum-flux-parametron (AQFP) circuits using an exact database. In: Proceedings of NANOARCH (2021)
23. Amarú, L., et al.: Enabling exact delay synthesis. In: Proceedings of ICCAD, pp. 352–359 (2017)
24. Calvino, A.T., Riener, H., Rai, S., Kumar, A., De Micheli, G.: A versatile mapping approach for technology mapping and graph optimization. In: Proceedings of ASP-DAC, pp. 410–416 (2022)
25. Mukhanov, O., Semenov, V., Likharev, K.: Ultimate performance of the RSFQ logic circuits. IEEE Trans. Magn. **23**(2), 759–762 (1987)
26. Soeken, M., et al.: Practical exact synthesis. In: Proceedings of DATE, pp. 309–314 (2018)
27. Zhang, H.-T., Jiang, J.-H.R., Amarú, L., Mishchenko, A., Brayton, R.: Deep integration of circuit simulator and SAT solver. In: Proceedings of DAC, pp. 877–882 (2021)
28. Marakkalage, D.S., Testa, E., Riener, H., Mishchenko, A., Soeken, M., De Micheli, G.: Three-input gates for logic synthesis. IEEE Trans. Comput. Aided Des. Integr. Circuits Syst. **40**(10), 2184–2188 (2020)
29. Amarú, L., Gaillardon, P.-E., De Micheli, G.: Majority-inverter graph: a novel data-structure and algorithms for efficient logic optimization. In: Proceedings of the Design Automation Conference (2014)
30. Katam, N.K., Pedram, M.: Logic optimization, complex cell design, and retiming of single flux quantum circuits. IEEE TASC **28**(7), 1–9 (2018)
31. Krylov, G., Friedman, E.G.: Asynchronous dynamic single-flux quantum majority gates. IEEE TASC **30**(5), 1–7 (2020)
32. Calvino, A.T., De Micheli, G.: Depth-optimal buffer and splitter insertion and optimization in AQFP circuits. In: Proceedings of ASP-DAC, pp. 152–158 (2023)
33. Leiserson, C.E., Saxe, J.B.: Retiming synchronous circuitry. Algorithmica **6**(1–6), 5–35 (1991)
34. Soeken, M., et al.: The EPFL Logic Synthesis Libraries. arXiv:1805.05121v3 (2018)
35. Benini, L., De Micheli, G.: A survey of boolean matching techniques for library binding. ACM Trans. Design Autom. Electr. Syst. **2**(3), 193–226 (1997)
36. Hansen, M.C., Yalcin, H., Hayes, J.P.: Unveiling the ISCAS-85 benchmarks: a case study in reverse engineering. IEEE Des. Test Comput. **16**(3), 72–80 (1999)
37. Yorozu, S., et al.: A single flux quantum standard logic cell library. Physica C: Superconductivity **378–381**, 1471–1474 (2002)
38. Amarú, L., Gaillardon, P.-E., De Micheli, G.: The EPFL combinational benchmark suite. In: Proceedings of IWLS (2015)